

# Steady streaming viscometry of Newtonian liquids in microfluidic devices

Giridar Vishwanathan and Gabriel Juarez\*

*Department of Mechanical Science and Engineering,  
University of Illinois at Urbana-Champaign, Urbana, Illinois 61801, USA*

(Dated: February 14, 2019)

We report a novel technique capable of measuring the kinematic shear viscosity of Newtonian liquids with steady streaming in microfluidic devices. This probe-free microrheological method utilizes sub-kilohertz liquid oscillation frequencies around a cylindrical obstacle, ensuring that the inner streaming layer is comparable in size to the cylinder radius. To calibrate the viscometer, the evolution of the inner streaming layer as a function of oscillation frequency for a liquid of known viscosity is characterized using standard particle tracking techniques. Once calibrated, we show how the steady streaming viscometer can be used to measure low-viscosity liquids and volatile liquids.

Steady streaming flows have received a renewed interest over the past decade due to their numerous applications in microfluidic devices [1, 2]. Here, steady streaming refers to the rectified flow [3] that occurs near the boundary of a rigid body of length-scale  $a$ , oscillating with frequency  $f$  and small-amplitude  $s$  ( $\ll a$ ), in a stationary incompressible fluid of kinematic viscosity  $\nu$ . The magnitude of the characteristic streaming velocity scales as  $U_s \sim \epsilon s \omega$ , where  $\epsilon = s/a$  is the dimensionless amplitude and  $\omega = 2\pi f$  is the angular frequency. At small scales, these rectified flows have been shown to be useful in non-contact manipulation [4], trapping [5–8], and sorting [9, 10] of particles and cells as well as in enhancing pumping [11] and mixing [12–14] at low Reynolds numbers. There are opportunities to use steady streaming for the rheology of liquids as well [15].

Microrheology aims at measuring local material properties of small quantities of fluids by studying the relationship between deformation and stress. Optical microrheology techniques rely on the tracking of flow tracers under passive thermal fluctuations or active external forcing [16–19]. The development of microrheological methods for complex fluids and soft materials [20, 21] has been motivated by the advantages offered by microfluidic devices compared to conventional bulk techniques, such as small sample volume, reduction of free-surface effects, direct visualization of the underlying microstructure, and the ability to quantify low-viscosity and weakly viscoelastic solutions [22, 23]. These specialized methods have been shown to measure material properties such as the steady shear viscosity [24], the most widely characterized material property, as well as the extensional viscosity [25, 26], and the longest relaxation time [27, 28] of various fluids.

Here, we aim to measure local material properties at the microscale, subject to independently controlled strain amplitude and frequency. We investigate the application of steady streaming for microrheology and experimentally demonstrate the measurement of kinematic shear viscosity of Newtonian liquids in microfluidic devices.

The steady streaming regime of an oscillating cylinder [29–31] is dictated by the magnitude of the Reynolds number,  $Re = \omega a^2/\nu$ , and the streaming Reynolds number,  $Re_s = \omega s^2/\nu$ . Microscale streaming flows and applications have previously focused on ultrasonic frequencies and above ( $f \geq 10$  kHz), typically induced by the interaction between a liquid and surface acoustic waves generated by piezoelectric transducers [1, 32]. The streaming regime associated with high frequencies and streaming Reynolds numbers greater than unity ( $Re_s > 1$ ) is that of a double streaming layer; an inner driving layer and an outer driven layer of the opposite sense. At high frequencies, the inner streaming region is confined to a thin layer near the cylinder surface making experimental studies of the inner region challenging and therefore less common [31]. By utilizing sub-kHz oscillation frequencies, our ex-

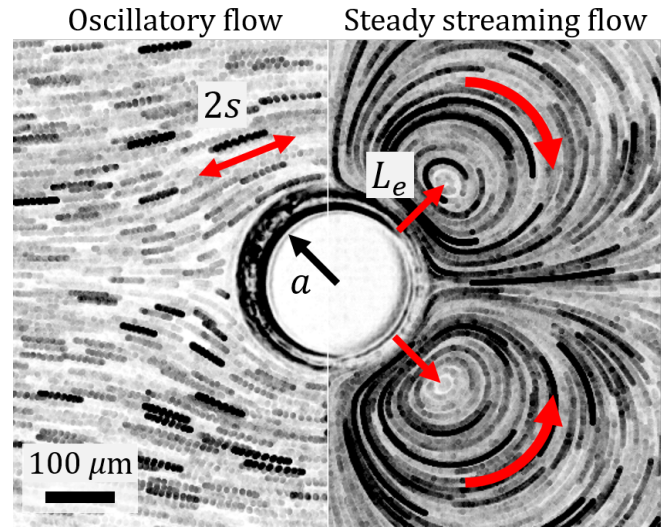


FIG. 1. Steady streaming in microfluidic devices. (Left) Pathlines of tracer particles captured with high-speed imaging. The displacement amplitude of  $2s$  is shown as the fluid undergoes one period of oscillation. (Right) Pathlines of tracer particles captured with stroboscopic imaging. Half of the steady streaming profile is shown with two counter-rotating vortices and the location of the eddy center,  $L_e$ . Here, the cylinder radius is  $a = 100 \mu\text{m}$ . See supplementary movies.

\* gjuarez@illinois.edu

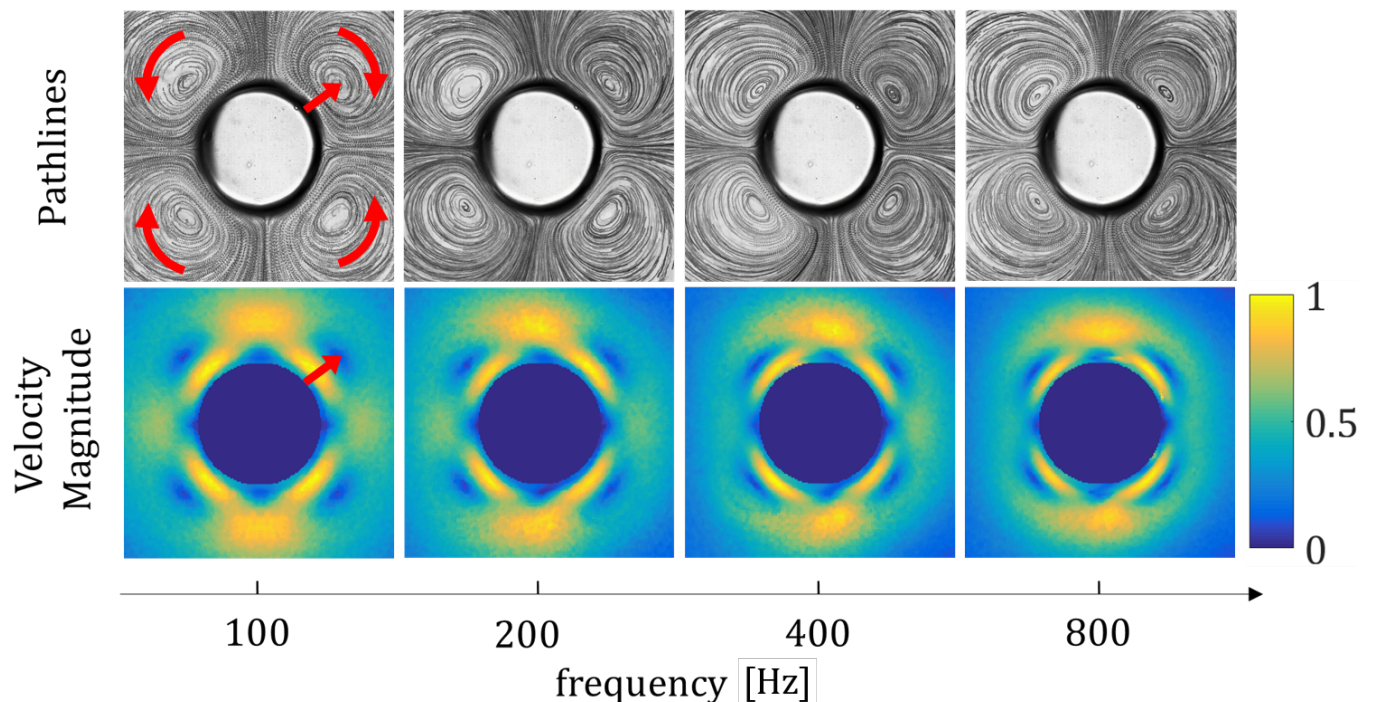


FIG. 2. Evolution of the steady streaming profile with increasing oscillatory frequency. (top) Pathlines of tracer particles captured with stroboscopic imaging showing the steady streaming profile around a cylindrical obstacle. The location of the eddy center moves closer to the cylinder boundary as the oscillation frequency is increased. (bottom) Normalized velocity field magnitude profiles obtained from particle tracking velocimetry (color online).

periments constrain the streaming Reynolds number to always be less than unity ( $Re_s < 1$ ), ensuring that the inner streaming layer is comparable in size to the cylinder radius. Because the inner boundary layer thickness scales as  $\delta \sim \sqrt{\nu/\omega}$ , our approach characterizes the evolution of the inner streaming boundary layer as a function of oscillation frequency with standard particle tracking techniques.

Experiments were performed in microfluidic devices molded in PDMS, consisting of a straight channel 20 mm long, 5 mm wide, and 200  $\mu\text{m}$  tall. Fixed cylindrical posts with radii  $a$  of 100, 200, 300, and 400  $\mu\text{m}$  were manufactured along the center of the straight channel. An electroacoustic transducer was used to externally drive the liquid in a microfluidic device. An oscillatory flow field,  $U(t) = U_\infty \cos(\omega t)$ , was setup in the channel over a range of frequencies  $40 \leq f \leq 1200$  Hz. The oscillation amplitude was independently controlled over a range of  $s \leq 100$   $\mu\text{m}$  such that all experiments were in the small-amplitude regime ( $\epsilon \ll 1$ ). The Reynolds number and the streaming Reynolds number correspond to a range of  $1 \leq Re \leq 1000$  and  $0.01 \leq Re_s \leq 1$ , respectively, for deionized water ( $\nu = 0.949 \times 10^{-6}$   $\text{m}^2/\text{s}$ ) over the entire frequency range investigated here.

Tracer particles, 0.93  $\mu\text{m}$  in diameter, were observed at the mid-height of the straight channel using bright field microscopy at 10 $\times$  and 20 $\times$  magnification. Images were acquired using CMOS cameras at sampling frequen-

cies greater than (high-speed) or at frequencies that are perfect divisors (stroboscopic) of the oscillatory flow frequency. High-speed imaging provided high fidelity observation of the oscillatory flow component while stroboscopic imaging was used to characterize the secondary streaming flow component. Experiments were performed at room temperature, maintained at 20  $^\circ\text{C}$ .

The oscillatory and steady streaming flow field of an incompressible Newtonian liquid near a PDMS cylinder of radius  $a$  is illustrated in Figure 1. The oscillation amplitude is determined from the pathlines of individual tracer particles undergoing a single period of oscillation located far from the cylinder, approximately  $5a$ , where the flow is uniform. An example of a minimum projection image, captured with high-speed imaging, shows the pathlines of tracer particles near the cylinder (Fig. 1, left). When viewed stroboscopically, the secondary steady streaming flow component, rather than the oscillatory flow component, is observed. The steady streaming flow has a quadrupolar structure, consisting of four counter-rotating vortices centered a distance  $L_e$  normal to the cylinder surface (Fig. 1, right). Flow is directed toward the cylinder boundary parallel to the oscillation direction and away from the cylinder boundary perpendicular to the oscillation direction (see supplementary movie).

The evolution of the steady streaming flow profile with increasing frequency for water is shown in Figure 2. The

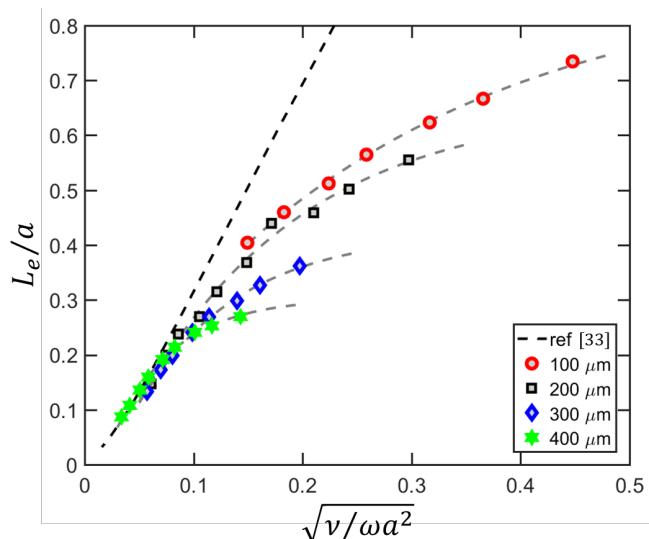


FIG. 3. Experimental measurements (symbols) of the nondimensional eddy center distance from the cylinder surface versus the nondimensional Stokes boundary layer for water. Calibration curves (grey dashed lines) for each cylinder radius are generated by fitting an exponential function to data points. Experiments converge to the analytical solution [33] (black dashed line) at high frequencies and large cylinder radii.

four counter rotating vortices are identified with tracer particle pathlines (Fig. 2, top row). The magnitude of the 2D velocity field, obtained using standard particle tracking velocimetry (PTV) routines [34], clearly shows the location of the central vortices with respect to the cylinder boundary (Fig. 2, bottom row). The eddy center location,  $L_e$ , decreases in magnitude and approaches the cylinder surface as the oscillation frequency is increased.

The dimensionless eddy center location increases monotonically with increasing dimensionless Stokes length (Fig. 3). In this case, the Newtonian liquid used was deionized water with  $\nu = 0.949 \times 10^{-6} \text{ m}^2/\text{s}$ . For small Stokes lengths ( $\sqrt{\nu/\omega a^2} \leq 0.1$ ), the dimensionless eddy center increases linearly, in good agreement with the theoretical treatment by Holtsmark et al. [33] (Fig. 3, black dashed line). For larger Stokes lengths ( $\sqrt{\nu/\omega a^2} \geq 0.1$ ), the location of the dimensionless eddy center diverges from the linear behavior and approaches a fixed value of  $L_e/a$ . The plateauing behavior, for values of  $\sqrt{\nu/\omega a^2} \geq 0.15$ , is attributed to the singular growth in the size of the dimensionless inner streaming layer [35]. As a consequence, the confinement effect of the device boundaries are felt very close to the cylinder, even for channel width to cylinder radii ratios of greater than 20. The plateau behavior is related to the channel width (in our case is fixed) to cylinder radius ratio and therefore largest for the  $100 \mu\text{m}$  cylinder and smallest for the  $400 \mu\text{m}$  cylinder.

Since the behavior was consistent for cylinders of different radii, calibration curves were generated by fitting an exponential function,  $L_e/a = A - B \exp(\sqrt{\nu/\omega a^2})$ , to the

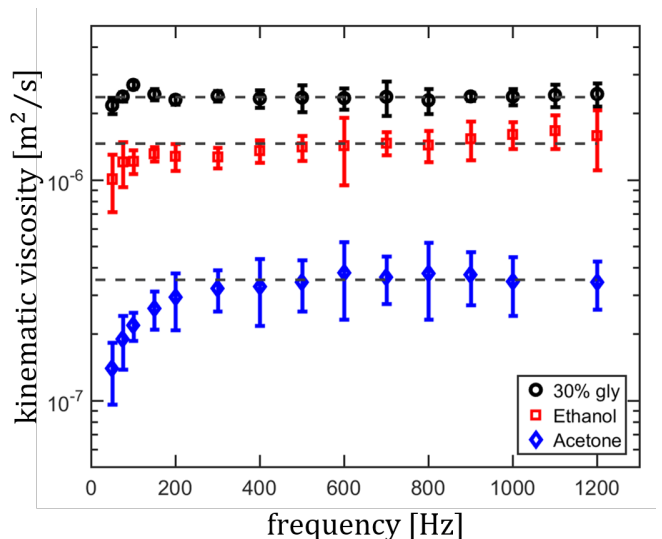


FIG. 4. Kinematic viscosity measurements of Newtonian liquids using steady streaming flows in microfluidic devices with a cylinder radius of  $200 \mu\text{m}$ . Dashed lines represent that average of individual values for frequencies greater than 300 Hz.

experimental data, where  $A/B$  is approximately unity (Fig. 3, grey dashed lines). Therefore, the kinematic viscosity of a Newtonian liquid can be determined by measuring the location of the dimensionless eddy center for given microfluidic device with cylinder radius  $a$  and angular frequency  $\omega$ . Microfluidic devices with a  $200 \mu\text{m}$  cylinder radius provided the largest dynamic range in measurements of  $L_e$  for the range of operation frequencies. Therefore, the  $200 \mu\text{m}$  radius cylinder was utilized for the measurements of the kinematic viscosity of Newtonian liquids.

The kinematic viscosity of three different Newtonian liquids was determined from the steady streaming profiles in microfluidic devices (Fig. 4). The Newtonian liquids used were acetone, ethanol, and an aqueous solution of 30% glycerol by weight. For frequencies greater than 200 Hz, the reported measurements of kinematic viscosity are approximately constant, or independent of oscillation frequency. Therefore, to obtain a single value of the kinematic viscosity, measurements for frequencies of 300 Hz and greater were averaged together.

The average values of kinematic viscosity are represented by grey dashed lines in Figure 4. The kinematic viscosity of acetone was measured to be  $3.52 \times 10^{-7} \text{ m}^2/\text{s}$ , which is within 12% of the expected value [36]. The kinematic viscosity of ethanol was measured to be  $1.48 \times 10^{-6} \text{ m}^2/\text{s}$ , which is within 2.6% of the expected value [37]. Finally, the kinematic viscosity of the 30% glycerol (w/w) solution was measured to be  $2.37 \times 10^{-6} \text{ m}^2/\text{s}$ , which is within 1.6% of the expected value [38].

The performance of our technique was compared against tabulated values of kinematic viscosity under similar temperature conditions [36–38]. The accuracy of our measurements ranged from within 2% to 12%, even for

volatile liquids, such ethanol and acetone. The largest discrepancy, in the case of acetone, was primarily due to evaporation and consequent bubble formation at the interface with the external driving mechanism. This caused secondary flows that interfered and distorted the inner streaming vortices resulting in relatively large error, particularly at frequencies less than 200 Hz.

In this work, we have demonstrated the use of steady streaming for microfluidic viscometry of Newtonian liquids. This optical microrheological technique implements independent and precise control of the liquid oscillation amplitude and frequency to maintain the streaming Reynolds number to be less than unity ( $Re_s \leq 1$ ). By utilizing sub-kHz frequencies, we characterize the evolution of the inner boundary layer as function of oscillation frequency with standard particle tracking and flow visualization techniques of different Newtonian liquids. For a given calibrated device, the kinematic viscosity is inferred.

Like other microrheological techniques, our method has similar advantages such as small sample volume, reduced surface effects, and a well-defined channel geometry. One additional advantage is a reduced measurement

time due to the short transient associated with the steady streaming viscometer, which is less than one second. While we used high-speed imaging and particle tracking techniques, they are not required to characterize the evolution of the inner streaming layer. Measurement of the eddy center location,  $L_e$ , can be determined from visualization of the tracer particle pathlines obtained from stroboscopic imaging (Fig. 1, right and Fig. 2, top row), making this technique accessible to those without a high-speed camera. Finally, a major advantage of this technique is the ability to quantify volatile and low-viscosity liquids that could be problematic with conventional bulk rheological methods. This technique could be useful in active microrheology of non-Newtonian fluids and further extended to investigate rate-dependent material properties and aging materials, such as viscoelastic liquids and biological fluids.

We want to thank Gwynn J. Elfring and Saverio E. Spagnolie for the invitation to present this work at the Banff International Research Station workshop, “Complex Fluids in Biological Systems”. We also want to thank Paulo E. Arratia for useful discussions and Jonathan B. Freund for feedback on the manuscript.

- 
- [1] J. Friend and L. Y. Yeo, *Reviews of Modern Physics* **83**, 647 (2011).
- [2] M. Wiklund, R. Green, and M. Ohlin, *Lab on a Chip* **12**, 2438 (2012).
- [3] N. Riley, *Annual Review of Fluid Mechanics* **33**, 43 (2001).
- [4] R. Amit, A. Abadi, and G. Kosa, *Biomedical Microdevices* **18**, 39 (2016).
- [5] P. Marmottant and S. Hilgenfeldt, *Nature* **423**, 153 (2003).
- [6] B. R. Lutz, J. Chen, and D. D. T. Schwartz, *Analytical Chemistry* **78**, 5429 (2006).
- [7] V. H. Lieu, T. A. House, and D. T. Schwartz, *Analytical Chemistry* **84**, 1963 (2012).
- [8] S. Yazdi and A. M. Ardekani, *Biomicrofluidics* **6**, 044114 (2012).
- [9] C. Wang, S. V. Jalikop, and S. Hilgenfeldt, *Applied Physics Letters* **99**, 034101 (2011).
- [10] R. Thameem, B. Rallabandi, and S. Hilgenfeldt, *Physical Review Fluids* **2**, 052001 (2017).
- [11] S. Girardo, M. Cecchini, F. Beltram, R. Cingolani, and D. Pisignano, *Lab on a Chip* **8**, 1557 (2008).
- [12] K. Sritharan, C. J. Strobl, M. F. Schneider, A. Wixforth, and Z. Guttenberg, *Applied Physics Letters* **88**, 054102 (2006).
- [13] B. R. Lutz, J. Chen, and D. T. Schwartz, *Analytical Chemistry* **78**, 1606 (2006).
- [14] D. Ahmed, X. Mao, J. Shi, B. K. Juluri, and T. J. Huang, *Lab on a Chip* **9**, 2738 (2009).
- [15] D. Vlassopoulos and W. R. Schowalter, *Journal of Non-Newtonian Fluid Mechanics* **49**, 205 (1993).
- [16] T. A. Waigh, *Reports on Progress in Physics* **68**, 685 (2005).
- [17] T. M. Squires and G. Mason, *Annual Review of Fluid Mechanics* **42**, 413 (2010).
- [18] L. G. Wilson and W. C. K. Poon, *Physical Chemistry Chemical Physics* **13**, 10617 (2011).
- [19] R. N. Zia, *Annual Review of Fluid Mechanics* **50**, 371 (2018).
- [20] C. J. Pipe and G. H. McKinley, *Mechanics Research Communications* **36**, 110 (2009).
- [21] T. A. Waigh, *Reports on Progress in Physics* **79**, 074601 (2016).
- [22] F. D. Giudice, S. J. Haward, and A. Q. Shen, *Journal of Rheology* **61**, 327 (2017).
- [23] F. D. Giudice, M. Tassieri, C. Oelschlaeger, and A. Q. Shen, *Macromolecules* **50**, 2951 (2017).
- [24] S. Gupta, W. S. Wang, and S. A. Vanapalli, *Biomicrofluidics* **10**, 043402 (2016).
- [25] F. J. Galindo-Rosales and M. A. Alves, *Microfluidics and Nanofluidics* **14**, 1 (2013).
- [26] S. J. Haward, *Biomicrofluidics* **10**, 043401 (2016).
- [27] F. D. Giudice, G. D’Avino, F. Greco, I. D. Santo, P. A. Netti, and P. L. Maffettone, *Lab on a Chip* **15**, 783 (2015).
- [28] J. Zilz, C. Schfer, C. Wagner, R. J. Poole, M. A. Alves, and A. Lindner, *Lab on a Chip* **14**, 351 (2014).
- [29] C.-Y. Wang, *Journal of Fluid Mechanics* **32**, 55 (1968).
- [30] K. Chong, S. D. Kelly, S. Smith, and J. Eldredge, *Physics of Fluids* **25**, 033602 (2013).
- [31] W. Coenen, *Proceedings of the Royal Society A* **472**, 20160522 (2016).
- [32] L. Y. Yeo and J. R. Friend, *Biomicrofluidics* **3**, 012002 (2009).
- [33] J. Holtsmark, I. Johnsen, T. Sikkeland, and S. Skavlem, *The Journal of the Acoustical Society of America* **26**, 26 (1954).
- [34] N. T. Ouellette, H. Xu, and E. Bodenschatz, *Experi-*

- ments in Fluids **40**, 301 (2006).
- [35] A. F. Bertelsen, Journal of Fluid Mechanics **64**, 589598 (1974).
- [36] K. S. Howard and F. P. Pike, Journal of Chemical and Engineering Data **4**, 331 (1959).
- [37] K. Soliman and E. Marschall, Journal of Chemical and Engineering Data **35**, 375 (1990).
- [38] *Physical properties of glycerine and its solutions* (Glycerine Producers' Association, New York, 1963).